

15

THE COSMIC X-RAY BACKGROUND

Elihu A. Boldt
Laboratory for High Energy Astrophysics
Goddard Space Flight Center
Greenbelt, Maryland 20771

1. OVERVIEW

Electromagnetic radiation provides the only channel presently available for obtaining direct information about extragalactic reaches of the universe; additional direct modes of making extragalactic observations (e.g., neutrino astronomy, gravitational radiation) are yet to be exploited. While most studies to date have concentrated on the individually discernible sources of this electromagnetic radiation, those absolute measurements of sky surface brightness providing the totality of the flux in various spectral bands from *all* sources in the universe (i.e., arising from diffuse emission as well as unresolved discrete objects) present us with a most fascinating and challenging constraint. This integrated radiation, known as the "background", gives us a quantitative measure for evaluating how complete our knowledge of the observable universe actually is. Fundamental questions may be posed. Does the total signal observed equal the sum of all the individual sources that we know about from limited samples? Do we have the correct arithmetic (i.e., cosmology) for carrying out this addition? Are there unfamiliar kinds of sources (e.g., with drastically different spectra) that contribute to the background substantially, but have not yet been resolved? What is the motion of our Milky Way galaxy relative to the proper frame of the background? With the advent of comprehensive data from the pivotal HEAO (High Energy Astronomy Observatory) program fostered by Frank McDonald and his associates [see history by Tucker,

1984], the cosmic X-ray background discovered by Giacconi et al. [1962] has now become a leading test case for attacking such questions.

Our present knowledge about the overall spectrum of the isotropic extragalactic background of electromagnetic radiation is summarized in Figure 1. It extends from radio frequencies below the turnover at about 6 MHz (i.e., wavelengths greater than 50 m) to gamma rays above the spectral break at several MeV (i.e., photon wavelengths smaller than 10^{-13} m). The power law observed in the radio band from about 10 MHz to 300 MHz [Clark, Brown, and Alexander, 1970], may be extrapolated to the high energy end of the spectrum [Boldt, 1971, 1974], merging remarkably well with the gamma ray background at a few hundred keV. The background above a few hundred keV may be accounted for in terms of the emission from Seyfert galaxies [Bignami et al., 1979; Boldt, 1981; Rothschild et al., 1983], with no appreciable contribution from sources at high redshifts ($z > 1$) required. In the X-ray band these sources exhibit power law spectra of energy index $\alpha = 0.7$ [Mushotzky, 1982], compatible with the index describing the power law connection of the background between radio frequencies and gamma rays (denoted by the dashed line in Figure 1). The observed spectral break in the gamma ray background at several MeV is taken to be indicative of a characteristic break in the spectra of Seyfert galaxies [Bignami et al., 1979]. The turnover in the radio background spectrum at about 6 MHz [Alexander and Clark, 1974] probably results from the combined effect of free-free absorption in the galactic disk, in the intergalactic medium, and in the sources themselves plus processes such as synchrotron self-absorption and Razin effect [Razin, 1960] in the individual sources. The power law portion of the radio background is well explained as the superposition of radio galaxies and other discrete radio sources [Simon, 1977], mainly associated with the present epoch ($z < 1$). Therefore, from radio to hard X-rays, we appear to have a unified power law background spectrum arising from the integrated contributions of nonthermal sources within the present epoch. This power law, extending over more than 14 decades in photon energy, serves as a baseline for examining additional background components of more limited bandwidth (e.g., "thermal bumps").

The isotropic extragalactic nonthermal radio background referred to above is in fact extracted from an anisotropic galactic background that dominates

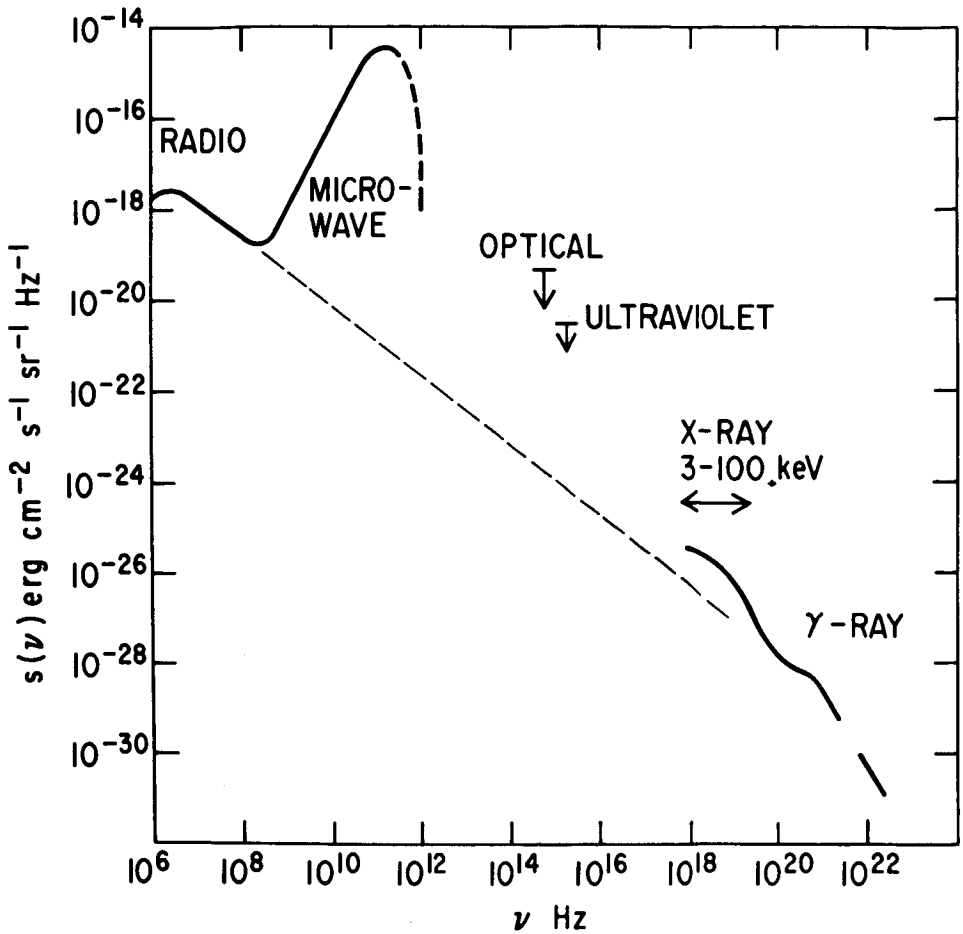


Figure 1. The isotropic sky flux $s(\nu)$ versus frequency ν [from Shafer, 1983]. The dashed line extends the power law spectrum at radio frequencies to higher photon energies ($E = h\nu$) assuming $s(\nu) \propto \nu^{-\alpha}$, with $\alpha = 0.7$. References are: Clark, Brown, and Alexander [1970] for radio; Weiss [1980] for microwave; Dube, Wickes, and Wilkinson [1979] for optical; Paresce, McKee, and Bowyer [1980] for UV; Marshall et al. [1980] and Rothschild et al. [1983] for X-rays; and Fichtel and Trombka [1981] for gamma rays.

the total flux. From about 1000 MHz to 10^6 MHz (0.3 mm wavelength), however, the situation changes drastically in that the sky is here dominated by an isotropic radiation field having the spectrum of a blackbody at 2.7 K [see review by Weiss, 1980], generally regarded as the cooled relic of the hot photon gas that dominated the universe after the initial few minutes [however, see Segal, 1983 for an alternate view]. At still higher frequencies (shorter wavelengths) we expect additional thermal components of the extragalactic background corresponding to dust (in the infrared [IR]), starlight (in the optical and ultraviolet [UV]) and possibly from hot gas (in the UV and extreme ultraviolet [XUV]). Upper limits to the extragalactic flux are shown in Figure 1 for the optical [Dube, Wickes, and Wilkinson, 1979; Code and Welch, 1982; Toller, 1983; Weller, 1983] and ultraviolet [Paresce, McKee, and Bowyer, 1980; Joubert et al., 1983]. In general, these upper limits are an order of magnitude higher than the flux anticipated from the superposed contributions of unevolved normal galaxies [Code and Welch, 1982]. Not until X-ray energies above 3 keV do we again encounter an isotropic background component that dominates the sky and where galactic contamination is negligible [for a description of the softer galactic component see McCammon et al., 1983]. This isotropic hard X-ray component extends out to almost 300 keV, appearing as a thermal-type bump well above the power law baseline shown in Figure 1. As pointed out by De Zotti [1982], the precision with which the spectrum of this cosmic X-ray background component has been measured with HEAO-1 [Marshall et al., 1980] exceeds that with which the cosmic microwave background spectrum has been defined. We examine some implications of the spectrum and (an)isotropy of this well-defined X-ray background within the context of individual source spectra, HEAO-2 "Einstein Observatory" source counts [Giacconi, this volume] and the dipole anisotropy of the microwave background. Open questions are emphasized.

2. ROLE OF THE HEAO PROGRAM

Although X-ray astronomy certainly flourished during the initial 15 years of its history, research on the cosmic X-ray background remained comparatively dormant. During this period, experiments concentrated on well isolated bright sources, particularly compact objects of high astrophysical interest, such as

neutron stars in binary stellar systems. However, there were also strong practical reasons for the relatively small attention given to the cosmic X-ray background during the early years of X-ray astronomy. With X-ray telescopes based on the mechanical collimation of photons, rather than focusing X-ray optics, it was not possible to detect any of the faint discrete sources contributing to the unresolved background [for a review of the early technical status see Giacconi, Gursky, and van Speybroeck, 1968]. Furthermore, all detectors used in X-ray astronomy suffer from an annoying background of signals arising from causes other than the X-ray sky; this extraneous background is the basic limiting factor in making the absolute measurements of surface brightness needed for properly defining the cosmic X-ray background. For discrete source measurements, even the “true” diffuse X-ray sky is an undesirable contamination. Hence, prior to the use of focusing X-ray optics, the standard approach was to make the mechanical collimation angle defining the detector aperture as small as practical and to simply measure the increase in signal as the instrument scanned across the discrete source of interest.

It remained for the High Energy Astronomy Observatories (HEAO-1 and HEAO-2) to significantly remedy the relatively poor observational situation that existed before concerning the X-ray background. The all-sky survey carried out over a broad band (from 0.1 keV to over 0.5 MeV) with the HEAO-1 mission (Frank McDonald, project scientist), launched in 1977, involved newly developed experiments especially designed to unambiguously distinguish the X-ray sky background from that due to other causes [Peterson, 1975; Boldt et al., 1979]. The focusing X-ray telescope flown on the HEAO-2 mission, usually known as the Einstein Observatory, brought the power of imaging optics to X-ray astronomy [Giacconi et al., 1979a]. For soft X-rays (< 3 keV), the imaging detectors at the focus of this grazing incidence telescope were used to resolve a substantial portion of the background into discrete faint sources [Giacconi et al., 1979b].

Some of the causes of the extraneous background associated with on-orbit X-ray detectors are charged cosmic rays, ambient electrons, gamma rays (primarily flux as well as a locally generated flux produced by cosmic ray interactions with the spacecraft), and radioactivity induced by passage through the South Atlantic Anomaly [Peterson, 1975]. The strategy for extracting the

diffuse flux of celestial X-rays from the overall background which was employed with the Cosmic X-ray Experiment (A2) on HEAO-1 [Boldt et al., 1979] is summarized as follows:

- (1) The most fundamental aspect of a diffuse flux is that it increases linearly with solid angle. In order to apply this definition reliably there were two different rectangular fields of view associated with each detector; one of them was always $3^\circ \times 3^\circ$, the dual one being $3^\circ \times 1.5^\circ$ for some detectors and $3^\circ \times 6^\circ$ for others (where the collimation angle transverse to the scan path was always 3°).
- (2) X-rays are detected via the photoelectric effect, which is a strong function of photon energy (i.e., the cross-section is roughly proportional to E^{-3} and changes at K absorption edges by an order of magnitude). To exploit this pronounced X-ray characteristic there were three classes of gas proportional counters, optimized for low, medium, and high energy X-rays, designated LED (low energy detector), MED, and HED respectively. Propane gas was used for soft X-rays (0.1-3 keV), argon for medium energy X-rays (1.5-20 keV), and xenon for hard X-rays (2-60 keV). [See detailed description by Rothschild et al., 1979.]
- (3) Unless there is a bright source in the detector's field of view, most of the raw signals generated by the sensor are due to penetrating charged cosmic ray particles that transverse the sensitive gas volume with a continuous trail of ionization. Since the electrons emerging from a photoelectrically ionized atom are of short range, the secondary ionization resulting from X-ray absorption is very localized. Hence, multi-anode veto logic could be used to efficiently reject cosmic ray signals without rejecting X-ray signals.
- (4) Ambient electrons associated with a low earth orbit (such as used for HEAO) are not as penetrating as cosmic rays and are relatively difficult to reject [Holt, 1974]. For a high energy gas proportional chamber, the main xenon-filled detector was separated from the entrance window by an electron sensing veto layer (propane-filled) transparent to hard X-rays. For the low energy detectors (propane-filled) this was not feasible

and deflection magnets were used for removing low energy electrons [effectiveness is described by Garmire, 1979].

- (5) Since the scan period of HEAO-1 (0.5 hour) was not small compared with the orbit period (1.5 hours) spatial and temporal effects needed to be separated; this was done by offsetting some of the detectors by an angle of only six degrees along the scan path.

The basic construction of a HEAO-1 (A2) proportional chamber involves an internal multi-wire electrode arrangement that is electrically equivalent to a rectangular stack of independent tubular "wall-less" counters, each with its own anode. X-rays enter via a mechanical collimator on top of the housing (see Figure 2), traverse a thin window and are detected in the multi-counter gas volume of the proportional chamber. The dual collimator is matched to the internal multi-counter structure of the proportional chamber; counters in odd numbered columns are aligned with the $3^\circ \times 3^\circ$ collimator while those in even numbered columns are aligned with the complementary collimator. A cross-sectional photograph of the MED dual collimator is shown in Figure 3 in order to indicate the cellular structure used to implement this scheme.

The HEAO-1 (A2) experiment consisted of six proportional chambers, two LED's for low energies, one MED for midband coverage, and three HED's for hard X-rays. To get some notion of how this experiment covered the sky we can examine the scan path on the celestial sphere for any one of the six detectors; this is shown in Figure 4. Every half-hour this dual collimator detector scanned a complete great circle on the celestial sphere in an angular band of 3° FWHM (full width at half maximum) normal to the HEAO spin axis. At any instant it viewed an angle θ (FWHM) along the scan path via those internal counters associated with the small collimation and an angle ($2 \times \theta$) via the dual portion of the instrument. The spin axis defining the scan plane pointed to the Sun, thereby moving one degree per day along the ecliptic equator. In this way the entire sky was scanned in six months.

The on-orbit performance of the dual collimator scheme is exhibited in Figure 5, where the effectiveness is quite evident. The two histograms displayed give the observed population distribution for count-rate samples sorted according

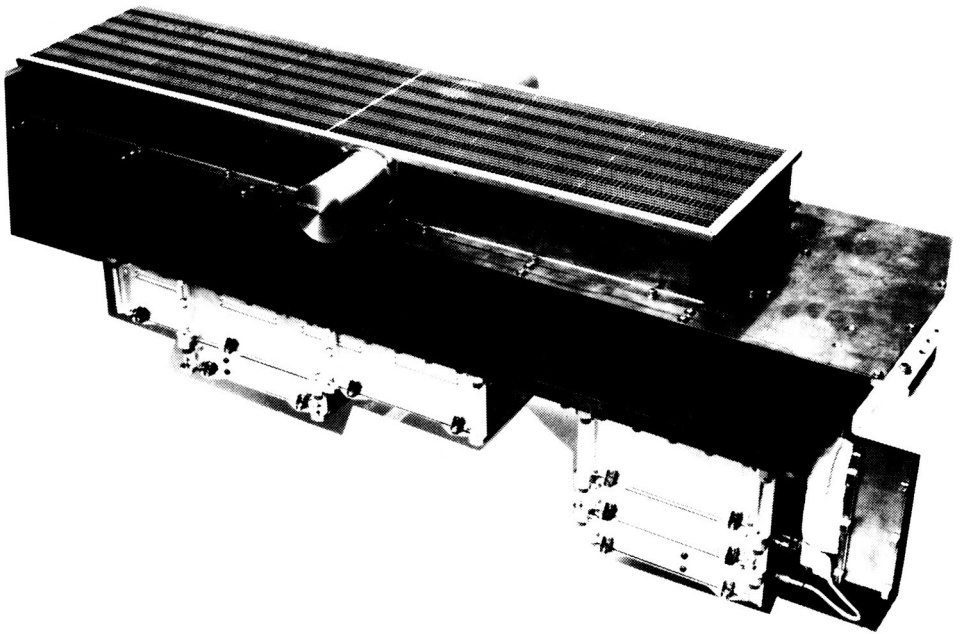


Figure 2. Photograph of a medium energy detector (MED) for the HEAO-1 (A2) experiment; overall length is about one meter. X-rays enter via mechanical collimator on top of housing. Boxes attached to bottom of detector housing are for associated electronics.

to the total number of accepted X-ray events per telemetry major frame (40.96s) recorded with HED-1. They are classified only with regard to field of view (FOV), the top histogram for counts associated with $3^\circ \times 6^\circ$ collimation and the bottom for counts associated with the $3^\circ \times 3^\circ$ collimation. These histograms are based on data obtained over many scan cycles regardless of what was in the field of view, be it Earth albedo or celestial sources. The histogram for each of the fields of view exhibits two clearly separated peaks, the high one attributed to exposures dominated by the sky and the one with lower counts attributed to exposures dominated by Earth albedo. If there were no extraneous sources of background the two histograms would scale as the

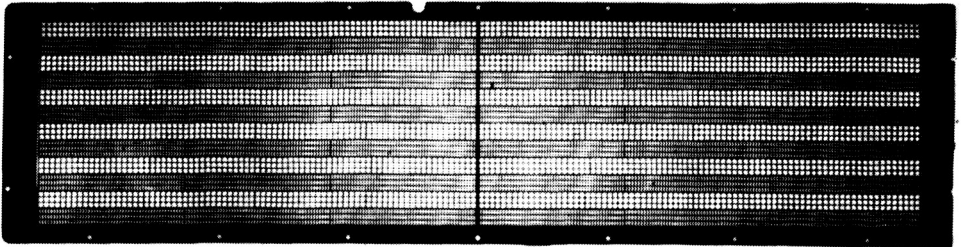


Figure 3. A cross-sectional photograph of the MED collimator showing cellular structure providing $3^\circ \times 3^\circ$ and $3^\circ \times 1.5^\circ$ dual collimation.

ratio of solid angles. In fact, Earth albedo represents a relatively weak source of X-ray surface brightness, even in the hard X-ray band considered here, and most of the signal when Earth fills the field of view arises from a residual background internal to the detector (i.e., due mainly to Compton electrons produced within the chamber by penetrating gamma rays). More extensive data bear out the qualitative indication in Figure 5 that the internal background to be associated with the two fields of view are equal, as expected. Furthermore, a detailed comparison of the internal background derived from the two peaks associated with diffuse sky background has been shown to be the same as that derived from the two peaks associated with Earth background, both in magnitude and spectral shape (i.e., using the relation: (Internal Background) = $2 \times$ (Small FOV) - (Large FOV)). As shown in Figure 5 by a dashed line, the internal background for HED-1 represents an average contamination of only about 14% for the large field of view, even when the full bandwidth (~ 60 keV) of this detector is considered. To exclude effects of internal background completely, however, the spectrum of X-rays to be associated with sky background was obtained by simply subtracting the raw spectrum observed with the small field of view from that obtained with the large field of view for the same detector.

At X-ray energies approaching 100 keV and above, the quantum efficiency obtained with gas counters is just not high enough and "tricks" of the sort

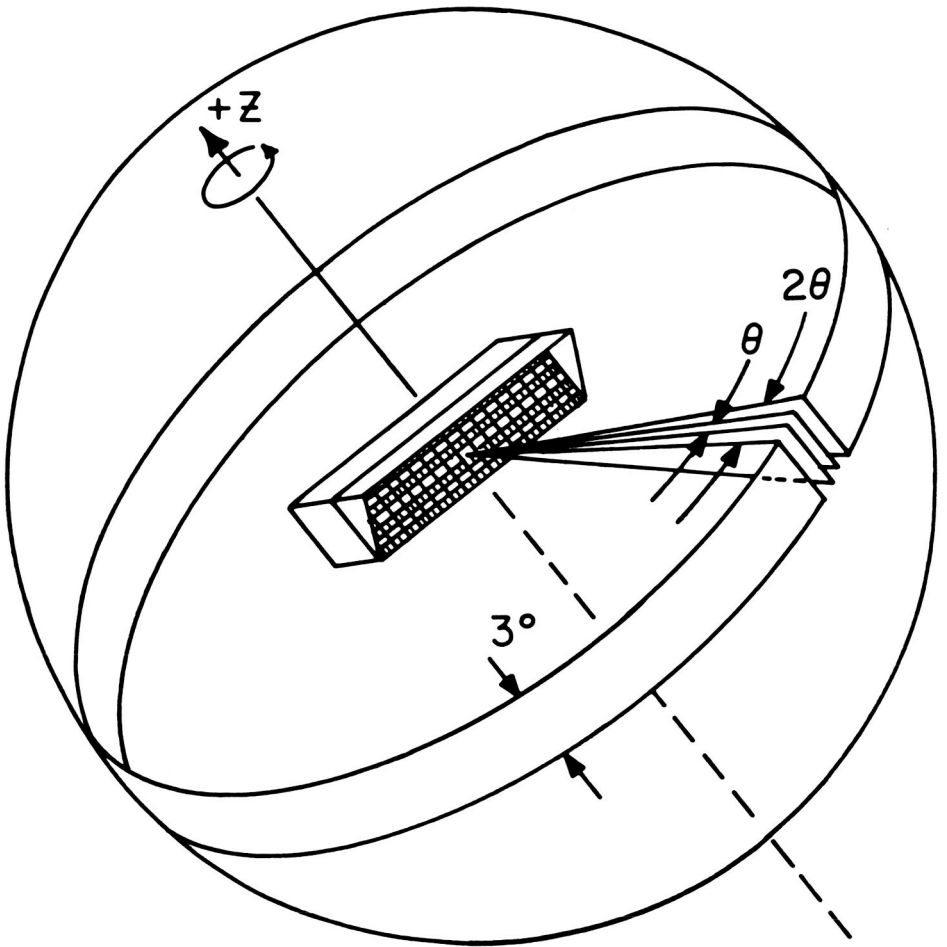


Figure 4. A schematic representation of the HEAO-1 celestial scan as depicted by one of the six (A2) detectors. The scan axis (z) always points to the Sun; as shown, each detector has a sun shade for shielding the collimator from solar radiation. The dual collimation angles along the scan path are indicated as θ and 2θ ; three detectors have $\theta = 1.5^\circ$ and three have $\theta = 3^\circ$.

NUMBER (N) OF SAMPLES OBSERVED:
DISTRIBUTED ACCORDING TO COUNT RATE (HEDI)

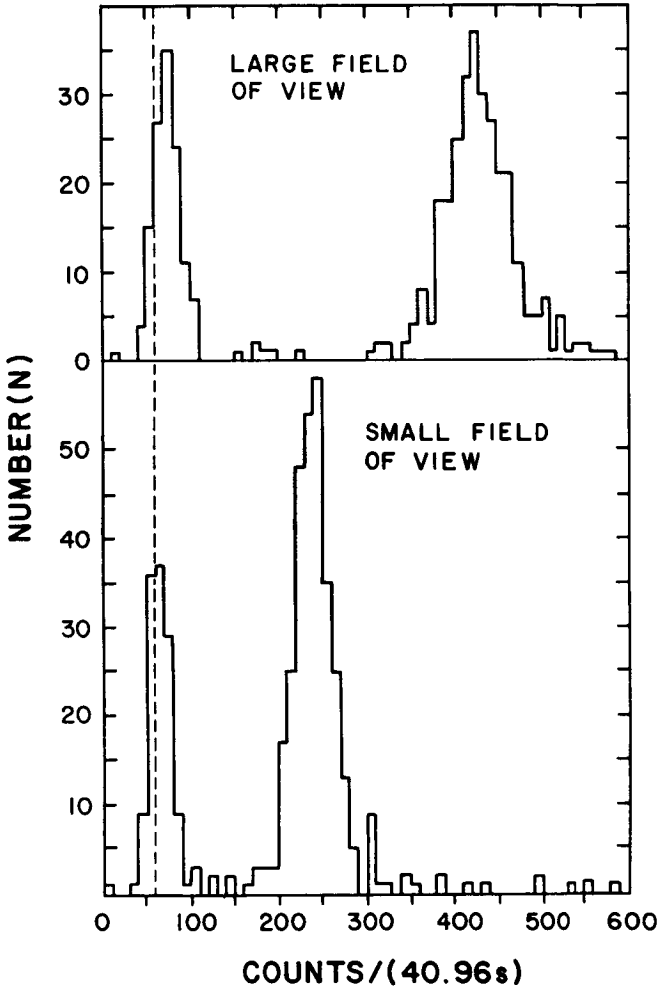


Figure 5. Histograms of sampled count rates sorted according to count per telemetry major frame (40.96 s) for HED #1 of HEAO-1 (A2), classified according to field of view (FOV)($3^\circ \times 6^\circ$ for the large FOV and $3^\circ \times 3^\circ$ for the small FOV).

used for the HEAO-1 (A2) experiment are no longer readily feasible. The detectors used for the HEAO-1 (A4) experiment for covering such high energy X-rays (and low energy gamma rays) involved an actively shielded layered configuration of solid scintillators (CsI(Na) and NaI(Tl)), where the light generated by one is distinguished from the other by the "phoswich" technique [Peterson, 1975]. After all the appropriate veto logic has been employed to reject many of the extraneous events, the rate of those still remaining due to causes other than the X-ray sky could be obtained by covering the detector aperture with a movable CsI(Na) scintillation crystal used in anti-coincidence with otherwise acceptable events. By accounting for the complication that the detector background depends on factors that vary in time (e.g., such as a cosmic ray flux and an induced radioactivity that vary with orbit phase) this procedure is used to estimate the absolute surface brightness of the X-ray sky at high energies [Gruber et al., 1984].

3. SPECTROSCOPY

The HEAO-1 (A2) experiment has been used to make spectral measurements of the extragalactic X-ray sky background that remains after excluding the brightest discrete sources resolved (i.e., on the order of 10 extragalactic objects per steradian). For high galactic latitudes, at $E > 3$ keV, the galactic contribution to this background is small and spectrally soft relative to the total [Iwan et al., 1982]. Employing the dual collimation scheme previously outlined, Marshall et al. [1980] determined that the spectrum of the absolute surface brightness of the extragalactic X-ray sky (3-50 keV) is well fitted by a model of optically thin thermal bremsstrahlung with $kT = 40$ keV. The scintillation detectors of the HEAO-1 (A4) experiment have been used to establish that this spectral model remains a remarkably valid description of the data up to about 100 keV [Rothschild et al., 1983; Gruber et al., 1984].

The CXB (Cosmic X-ray Background) presents us with a pronounced spectral paradox when regarded as the superposition of the contributions from discrete extragalactic sources corresponding to known classes of objects. While the majority of the extragalactic sources detected with the HEAO-2 Einstein Observatory are probably AGN (Active Galactic Nuclei) such as Seyfert galaxies and quasars [Gioia et al., 1984] the broadband continuum for the brightest

of such objects measured with HEAO-1 exhibit spectra quite different from that of the CXB. As displayed in Figure 6, these AGN exhibit power law spectra characterized by an energy spectral index value distributed in a narrow interval about $\alpha = 0.7$, apparently independent of classification or luminosity [Mushotzky, 1982]. Such a power law fails to fit the spectrum of the CXB, being clearly too steep below 10 keV and much too flat above 20 keV (see Figure 7). In general, the bright AGN observed with HEAO-1 are within the present epoch (i.e., low redshift). As shown in Figure 8, the composite broadband spectrum for a dozen of the brightest of these is well represented by a single power law up to 100 keV [Rothschild et al., 1983]. While a power-law model for the CXB spectrum is possible with $\alpha = 0.4$ over a limited band below 10 keV, it is too flat at higher energies (see Figure 7). An extrapolation of the steeper power law spectrum characterizing the contribution of unevolved Seyfert galaxies, however, could well account for essentially all of the background at energies above a few hundred keV provided there is an eventual gamma ray fall-off at several MeV [see Figure 9, taken from Rothschild et al., 1983]. Of course, the very pronounced residual CXB in the band below 100 keV of interest here remains to be explained.

Extrapolating from the sample of sources detected with the HEAO-2 Einstein Observatory, Maccacaro, Gioia, and Stocke [1984] deem it plausible to consider that most of the residual CXB could be due to quasars. Although many quasars have been observed in X-rays with HEAO-2, the data are restricted to energies below 3 keV and spectral determinations are relatively uncertain [Elvis, Wilkes, and Tananbaum, 1985]. Furthermore, even assuming that the residual CXB is indeed dominated by discrete objects (i.e., not diffuse), most such sources would be too faint to have been resolved. Hence, at this stage the spectrum characteristic of the ensemble of sources that dominate the residual CXB can only be inferred from the spectrum of the CXB itself. More precisely, we must account for that portion of the CXB arising from sources of known spectral properties (such as those observed within the present epoch) in order to isolate the residual CXB to be identified with faint discrete sources (e.g., at very large redshifts) and/or a diffuse mechanism. This has been done under a variety of approximations [De Zotti et al., 1982; Leiter and Boldt, 1982; Worrall and Marshall, 1984; Schmidt and Green, 1986], all consistent with the same general picture emerging. Specifically, the sources of the residual CXB are in this way found to be

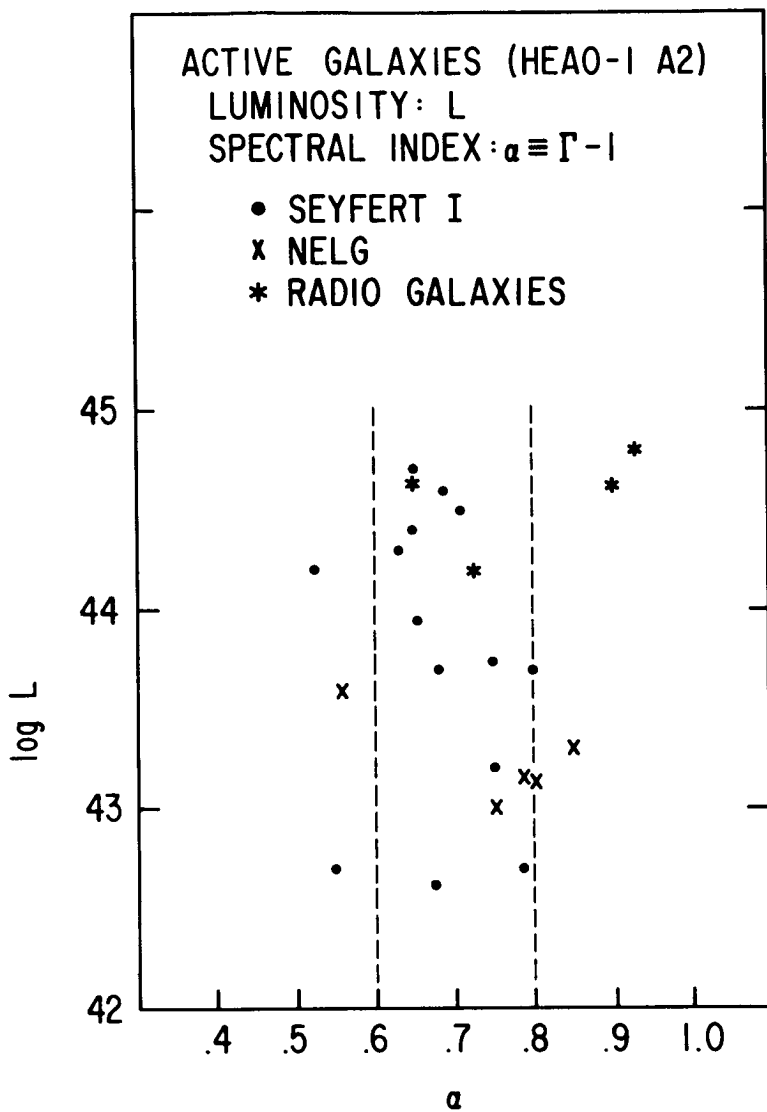


Figure 6. Active galaxies measured with the HEAO-1 (A2) experiment [Mushotzky, 1982] plotted with regard to X-ray luminosity (L ergs s^{-1}) below 20 keV and energy spectral index α .

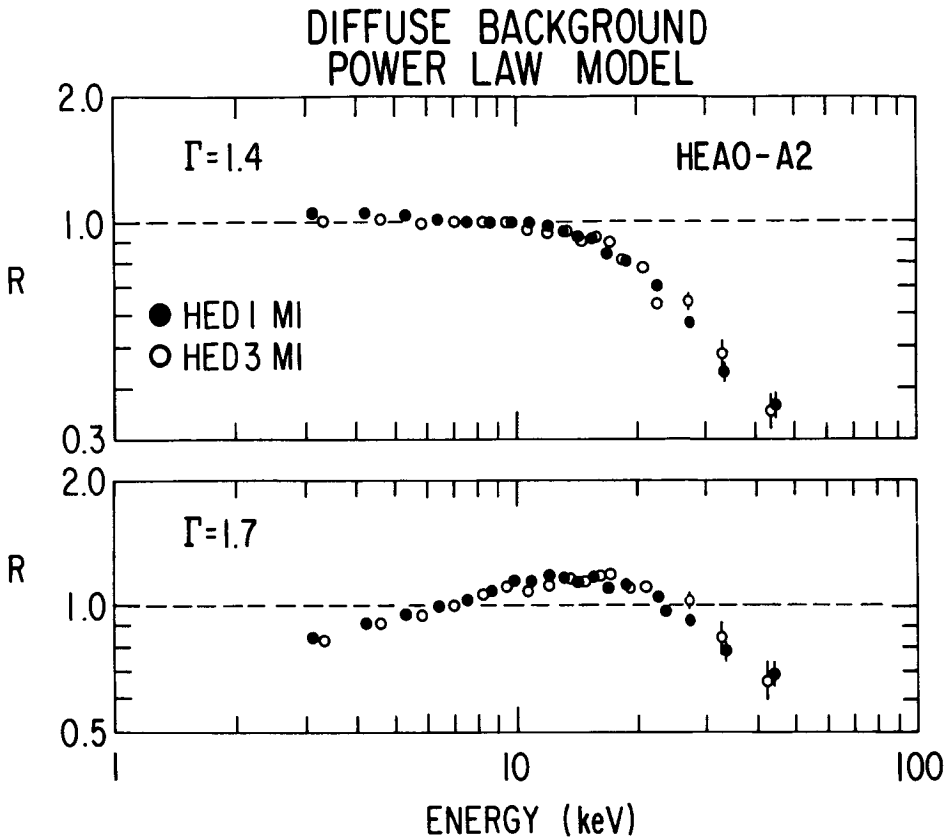


Figure 7. The ratio (R) as a function of energy of the counts observed for the X-ray background to that predicted by convolving, with the detector response function, power law spectra characterized by photon number spectral indices $\Gamma = 1.4$ and $\Gamma = 1.7$. Different symbols distinguish data obtained with HED-1 and HED-3 detectors of HEAO-1 (A2). Statistical errors are shown when larger than the size of the symbols [Marshall et al., 1980].

characterized by spectra that are extremely flat at the lowest energies and then fall off with an e-folding energy of $B(1+z)$ in their proper frame, where $B = 23 \rightarrow 30$ keV [Leiter and Boldt, 1982] and z is redshift. For $z \gtrsim 3.5$,

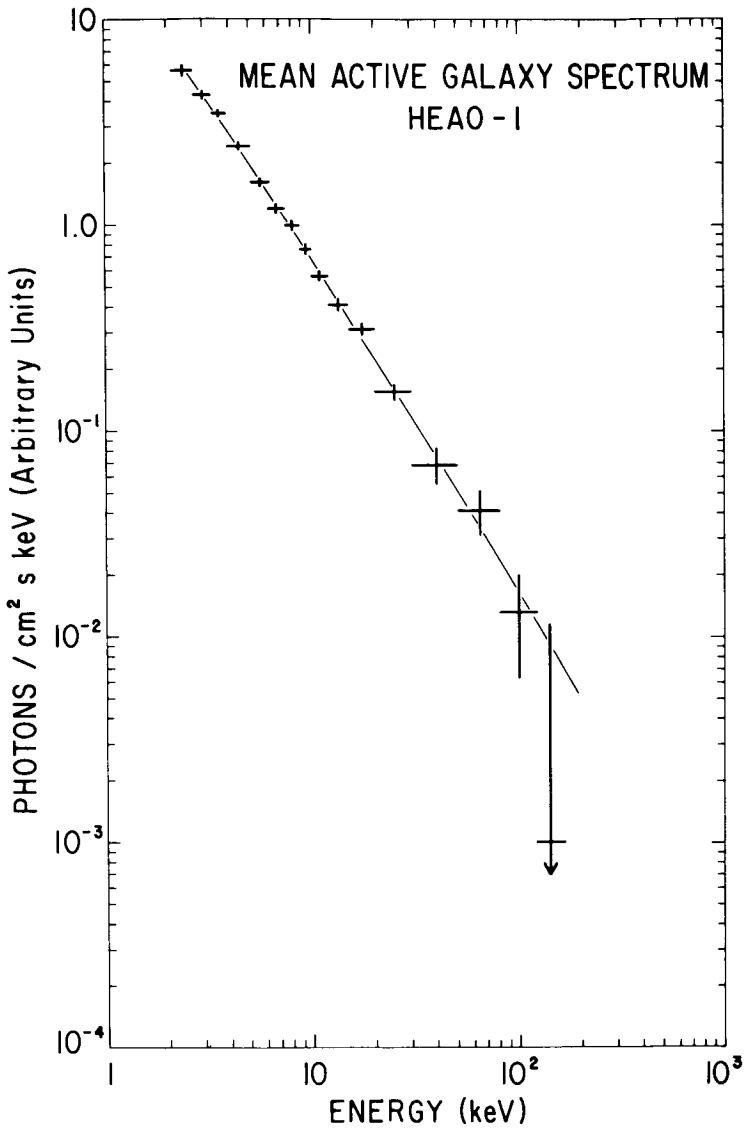


Figure 8. The mean spectrum obtained for a sample of bright AGN observed with the HEAO-1 (A2) and (A4) experiments [Rothschild et al., 1983]. The solid line is the best-fit power law model.

ORIGINAL PAGE IS
OF POOR QUALITY

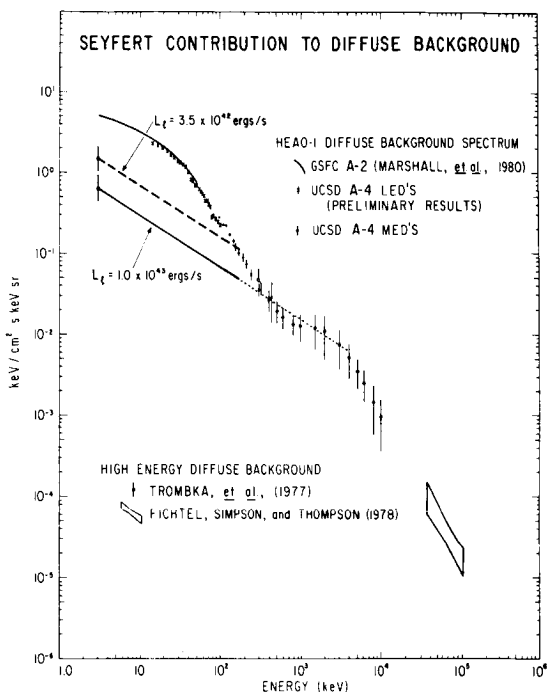


Figure 9. The Seyfert galaxy estimated contribution to the diffuse background, along with the HEAO-1 diffuse X-ray background 3-400 keV, plus points from 300 keV to 10 MeV [Trombka et al., 1977] and from 35 to 100 MeV [Fichtel, Simpson, and Thompson, 1978]. The dashed line represents the 2-165 keV power law spectra contribution from active galaxies under the assumption of a low luminosity cutoff at 3.5×10^{42} ergs s^{-1} [for a single power law luminosity function of index 2.75; see Piccinotti et al., 1982]. The solid line represents the contribution under the assumption of a break in the luminosity function index of one at 1×10^{43} ergs s^{-1} . The dotted line is an extension of the model to 4 MeV to guide the eye. The error bars at the beginning of the dashed and solid lines represent the uncertainty in the intensities due to uncertainties in the luminosity function. LED stands for the 12-165 keV Low Energy Detector, and MED stands for the 80-400 keV Medium Energy Detectors of the UCSD/MIT A-4 experiment [Rothschild et al., 1983]. The curve shown for the background (3-40 keV) is the best-fit to data obtained with the GSFC detectors of the A-2 experiment [Marshall et al., 1980].

where there is an apparent paucity of canonical quasars [Osmer, 1982; Schmidt and Green, 1983], this characteristic energy would be somewhat greater than 100 keV.

The 3-100 keV “thermal” spectrum of the overall extragalactic sky (i.e., before removing any estimated contributions from unresolved “foreground” sources) may be approximated by the following expression:

$$dI/dE = A [E/(3 \text{ keV})]^{-\alpha} \exp(-E/B)$$

where E is photon energy (in keV), $A = 5.6 \text{ keV}/(\text{keV cm}^2 \text{ s sr})$, $B = 40 \text{ keV}$ and $\alpha = 0.29$. This is to be contrasted with the broadband spectra for individually resolved sources in the present epoch. We here characterize these known discrete source spectra in terms of the same spectral form used above for the overall CXB. Accordingly, the ensemble average spectrum for clusters of galaxies may be described by an optically thin thermal model fixed by $B = kT = 7 \text{ keV}$ [Stottlemyer and Boldt, 1984], and $\alpha = 0.4$; however, the contribution of such clusters is only a few percent [McKee et al., 1980]. Low redshift AGN such as Seyfert galaxies make a much more substantial contribution to the CXB (see Figure 9) and, for the brightest observed, have spectra characterized by $\alpha = 0.7$ [Mushotzky, 1984] and $B > 100 \text{ keV}$ [Rothschild et al., 1983]. Considering 25 quasars brighter than visual magnitude 16 (with mean redshift $z = 0.37$), Worrall and Marshall [1984] have correlated data from HEAO-1 (A2) and HEAO-2 to obtain that the broadband spectrum of the ensemble may be characterized by an energy spectral index $\alpha = 0.8(+.3, -.2)$. Although the spectrum for this ensemble of quasars (mostly radio-loud) is compatible with that for Seyfert galaxies there is now some evidence from HEAO-2 that the low energy spectra ($E < 3 \text{ keV}$) for quasars in a true optically selected sample are somewhat steeper [Elvis, 1985]. Steeper AGN spectra such as these would further aggravate the discrepancy with the CXB spectrum below 10 keV already noted for Seyfert galaxies.

Taking $\alpha = 0.6 \rightarrow 0.9$ for AGN and $B = 7 \text{ keV}$ for clusters of galaxies, the foreground spectrum arising from the composite of all these sources has been estimated [Leiter and Boldt, 1982, Appendix D]; with the normalization adopted, it amounts to 30% of the CXB over the band 3-10 keV. Subtracting this foreground from the spectrum of the overall CXB yields that of the residual

CXB which we may use for characterizing those extragalactic sources yet to be identified. As shown in Figure 10, for $E < 10$ keV this residual background is clearly flatter than that of the total CXB. For $E \gg 40$ keV, we expect that Seyfert galaxies will dominate the total background [Bignami et al., 1979; Boldt, 1981; Rothschild et al., 1983], with the residual CXB becoming relatively small [see discussion of spectral model by Leiter and Boldt, 1982]. In terms of the spectral form used here the residual CXB itself must have $\alpha < 0.2$ and $B = 23 \rightarrow 30$ keV. As shown in Figure 11 a good fit is obtained with $\alpha = 0$ and $B = 23$ keV. The main sources of the residual CXB should exhibit such a spectrum.

The spectrum for optically thin thermal bremsstrahlung by a hot Maxwellian plasma may be well approximated (over the band 3-100 keV) by an expression of the form used above for the CXB. In particular we note [Maxon, 1972] that $\alpha = 0.19$ for $kT = B = 200$ keV. Hence, the requirement that $\alpha < 0.2$ for the residual CXB (as viewed by the observer) implies $kT > 200$ keV at the sources of emission. Under the condition $B = 23 \rightarrow 30$ keV for the observed redshifted spectrum these sources would have to be located at $z > 6$ (i.e., well beyond any known quasar). While "protogalaxies" rich in supernovae at high redshifts could well yield hot X-ray emitting galactic winds, the anticipated temperature [Bookbinder et al., 1980] might not be hot enough. Galaxy formation in an IGM (intergalactic medium) dominated by explosions, however, might give rise to a suitably hot phase [Ostriker and Cowie, 1981]. As emphasized by Fabian [1981], heating of the IGM to $kT > 200$ keV at high redshifts could provide a "natural" explanation for the spectrum of the residual CXB. According to this scenario [Guilbert and Fabian, 1986], the IGM is heated at a redshift $z < 6$ to an energy density about 40% of that in the microwave background; it initially cools mainly via Compton scattering with the microwave background (for $z > 3.5$) and subsequently cools by adiabatic expansion, decreasing in temperature to $kT < 20$ keV after a Hubble time. Between 20% and 50% of the closure density of the universe would be in this hot IGM; it would contain most of the baryons in the universe. The cosmological implications of the hot IGM hypothesis are obviously very important. While reducing the absolute magnitude of the residual CXB (i.e., increasing the level estimated for the foreground power law spectrum attributed to unresolved AGN) would mitigate the severe cosmological confrontation

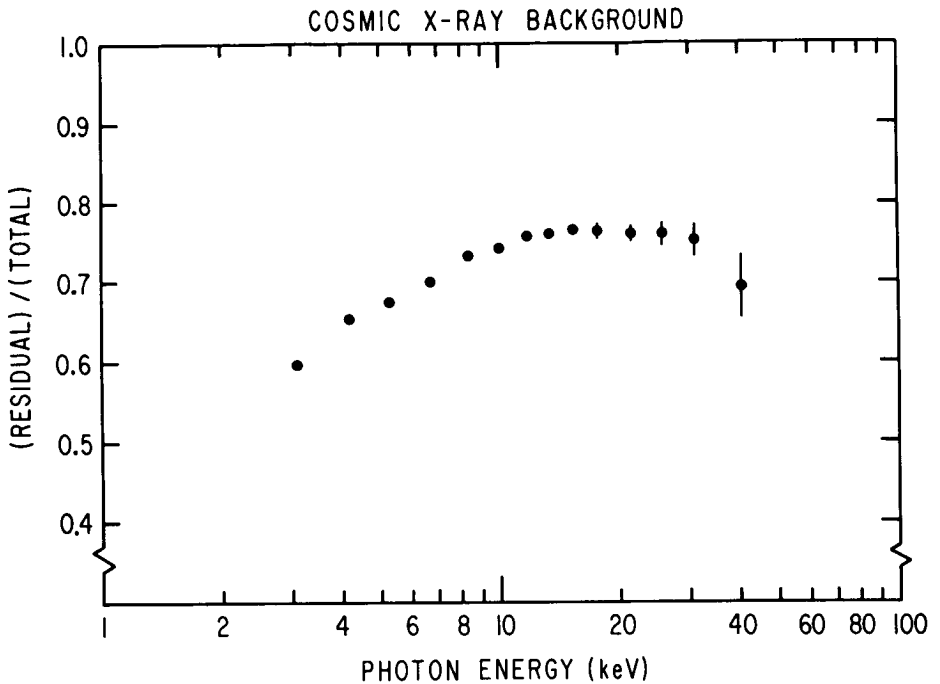


Figure 10. The ratio of the spectral density of the estimated residual CXB [Leiter and Boldt, 1982] to that of the total CXB observed with HEAO-1 (A2), plotted as a function of photon energy, in keV. Statistical errors are indicated for those data points where they exceed the size of the dots.

involved with this model, it would in fact destroy the amazingly good spectral agreement achieved with it over a broad bandwidth.

If we assume that the CXB is dominated by the integrated contributions of AGN in all their various stages of evolution, then the residual CXB spectrum may be used as a constraint on the as yet unresolved sources indicative of the youngest AGN (i.e., those of highest redshift). For example, based on

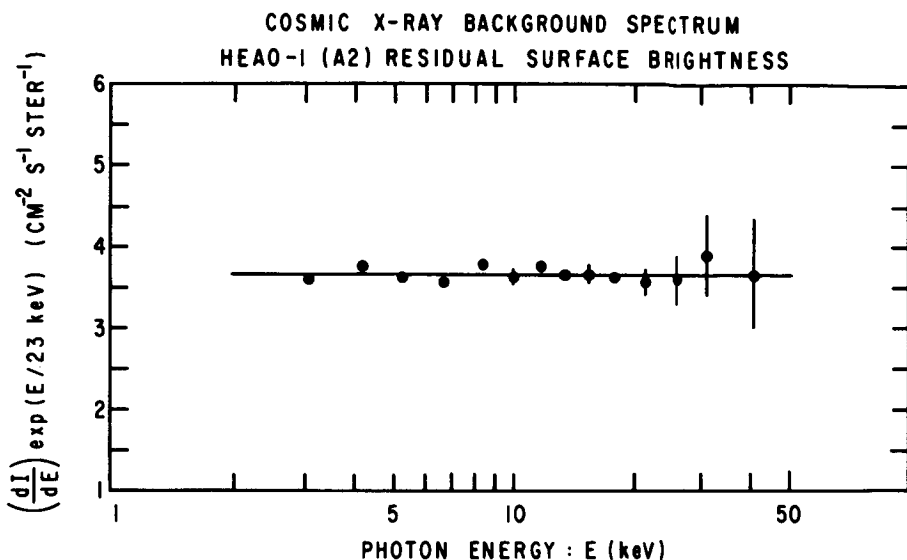


Figure 11. The residual energy spectrum for the CXB multiplied by $\exp(E/23 \text{ keV})$ as a function of photon energy [Leiter and Boldt, 1982]. In general, the statistical errors associated with the data points increase with energy and are indicated only for representative energies ($\sim 5 \text{ keV}$, 10 keV and $> 20 \text{ keV}$).

a model of black hole disk accretion [Leiter and Boldt, 1982], a picture emerges in which:

- (1) Young AGN emission occurs mainly in the X-ray band, arising from highly compact sources (i.e., a few times the gravitational radius of the central supermassive black hole in size) radiating at the Eddington luminosity limit.
- (2) Canonical AGN represent later stages (less compact) exhibiting a broadband power law spectrum extending to the gamma ray regime.

Young AGN characteristic of the residual CXB could then be relatively weak optical sources [Boldt and Leiter, 1984], possibly explaining the apparent paucity of canonical quasars at $z > 3.5$. The hot, optically thin, inner disk X-ray

emission characteristic of young AGN would be diminished at a later stage, but optically thick radiation from a cooler disk may explain the "UV bump" observed for AGN [Malkan and Sargent, 1982]. In a similar sense, the residual CXB that appears above the broadband nonthermal continuum spectrum of the overall background (see Figure 1) may be viewed as indicative of a "thermal bump" dominating the emission of *young* AGN.

In our discussions interpreting the residual CXB we have implicitly assumed that the background observed is the superposition of radiation coming directly from all the sources of emission in the universe. This is the kind of arithmetic prescribed by any standard cosmology which excludes the possibility of a cosmological albedo due to the entire universe in which all the sources are embedded. With Friedmann cosmology, which is not temporally homogeneous, once radiation is emitted it propagates away never to return. In any temporally homogeneous model based on a closed space, however, the radiation may circulate many times around before it is scattered or absorbed [Segal, 1985]. As viewed by Segal [1983] the microwave background could thereby be intrinsically diffuse cosmological albedo arising from dust. If such is the case, then the cosmological albedo responsible for the residual CXB would probably be due to Compton scattering from gas and plasma. Because of radiative transfer effects associated with Compton scattering such an albedo would occur mainly at energies less than mc^2 , explaining the possible absence of any significant amount of genuinely diffuse background above a few hundred keV.

4. ISOTROPY

When viewed over large angular scales at high galactic latitudes the CXB is essentially isotropic [Boldt, 1981; Shafer, 1983; Shafer and Fabian, 1983]. A small global anisotropy observed in the overall background (> 3 keV) is due mainly to our galaxy. This galactic component accounts for about 2% of the background at high latitudes; characterized by $kT = 9$ keV its spectrum is softer than that of the CXB [Iwan et al., 1982]. The observed small-scale fluctuations of CXB surface brightness may be ascribed to statistical variations in the population of unresolved discrete sources [Shafer, 1983] among the pixels examined. The number-flux relation ($N \propto S^{-1.5}$) for the bright extragalactic X-ray sources (> 3 keV) observed with HEAO-1 [Piccinotti

et al., 1982] may be extrapolated to the regime of unresolved faint sources needed for evaluating such fluctuations. Assuming typical source spectra, this extrapolation is consistent with the number-flux relation for faint sources directly obtained [Gioia et al., 1984] from HEAO-2 observations (< 3 keV). The apparent surface brightness fluctuations arising from those sources in this population unresolved with HEAO-1 are found to be statistically consistent with the variations observed [Shafer, 1983]. The upper limit to any residual variations implies that sources fainter than those already detected in the HEAO-2 deep survey [Giacconi et al., 1979b] can make only a relatively small contribution to the total fluctuations. Assuming an energy spectral index $\alpha = 0.7$, the flux threshold $S_0(1-3 \text{ keV}) = 2.6 \times 10^{-14} \text{ ergs cm}^{-2} \text{ s}^{-1}$ for the source sample obtained in this deep survey corresponds to $S_0(3-10 \text{ keV}) = 4.0 \times 10^{-14} \text{ ergs cm}^{-2} \text{ s}^{-1}$. With this scaling, the population of sources represented by the HEAO-2 sample accounts for only $18(+7, -7)\%$ of the CXB (3-10 keV). Hence, it is evident that the CXB flux itself must be dominated by sources other than those responsible for most of the fluctuations. This means that the number of sources fainter than the HEAO-2 deep survey limit must be relatively high [Shafer, 1983] or that the CXB is largely diffuse.

Models for the origin of the CXB attribute it to numerous, weak, unresolved discrete sources (e.g., low luminosity AGN, as discussed by Elvis, Soltan, and Keel, 1984), to some diffuse mechanism (e.g., thermal bremsstrahlung from a hot IGM), or to an unresolved population of discrete sources which evolve substantially with redshift (e.g., quasars). Turner and Geller [1980] have shown that comparison of the CXB surface brightness variations with flux variations in the integrated light from galaxies can measure the relative contributions of these possible sources of the CXB. Applying the technique to Uhuru data, they find that the absence of correlation between the optical flux variations and the X-ray flux variations sets an upper limit of about 50% on the fraction of the CXB originating with any classes of X-ray sources substantially represented among bright ($m_{pg} < 15.5$) galaxies. The data are consistent with nearly all of the CXB being due to diffuse emission or to a class of sources whose density and/or luminosity increases rapidly with redshift. Further studies of such correlations (or limits on them) are being carried out with HEAO-1 (A2) data on the CXB [Persic et al., 1986], including a direct

comparison with the infrared sky as observed with the IRAS (Infrared Astronomy Satellite).

Since the HEAO-1 mission surveyed the sky with scan paths that follow great circles which always traverse the ecliptic poles, the most straightforward and reliable way to investigate possible weak global anisotropies of the CXB involves referring data to ecliptic coordinates. Figure 12 shows the geometry to be considered, expressed in ecliptic coordinates; latitude is β , longitude is λ . In this representation, supplementary longitudes λ and $(\lambda + 180^\circ)$ are used to identify the dual traces of any given great circle scan path. The loci of galactic and supergalactic equator crossings are shown by the curves labeled as such. Some specific directions of particular interest cluster together in the general vicinity of $\lambda = 180^\circ$ and are separately identified by numbers, as follows:

- #1 (at $\lambda = 185^\circ$) gives the direction of the dipole anisotropy characteristic of the microwave background, as measured by Smoot, Gorenstein, and Muller [1977].
- #2 (at $\lambda = 164^\circ$) gives the direction of the microwave dipole anisotropy, as measured by Cheng et al. [1979].
- #3 (at $\lambda = 184^\circ$) gives the direction of the Virgo Cluster near the center of the Supergalaxy [de Vaucouleurs, 1958].
- #4 (at $\lambda = 170^\circ$) is the solar velocity direction relative to distant galaxies [Hart and Davies, 1982] and, within errors, is consistent with the preferred direction for the microwave background.

The preferred direction to be associated with the microwave background is close to the ecliptic equator, which makes the investigation of correlations particularly well suited to studies carried out with HEAO-1. To minimize galactic effects (i. e., by avoiding appreciable variations of galactic latitude relative to this direction) only those data corresponding to a band within 24° of the ecliptic equator are considered here; this band is outlined on Figure 12 with dashed lines. Even so, unavoidable galactic effects do become important when considering longitudes close to where the galactic equator crosses the ecliptic

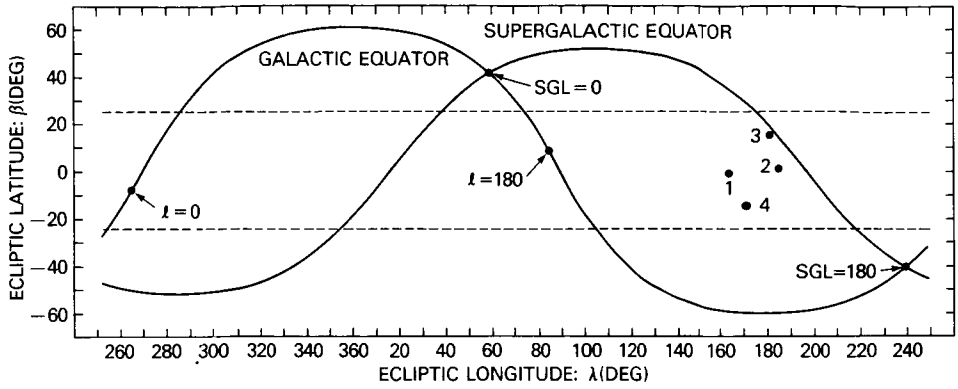


Figure 12. Special directions on the celestial sphere, expressed via ecliptic coordinates, in degrees (latitude: β , longitude: λ). The galactic and supergalactic equators are indicated by solid curves. The galactic center and anti-center are denoted by galactic longitudes $l = 0$ and $l = 180^\circ$, respectively. Reference supergalactic longitudes are denoted by $SGL = 0$ and $SGL = 180^\circ$. The dashed lines outline the band within 24° of the ecliptic plane used for evaluating anisotropies (see text). #1 ($\lambda = 185^\circ$) and #2 ($\lambda = 164^\circ$) indicate the direction of the dipole anisotropy of the microwave background as determined by Smoot et al. [1977] and Cheng et al. [1979], respectively. #3 ($\lambda = 184^\circ$) is the direction of the Virgo Cluster and #4 ($\lambda = 170^\circ$) is the direction of the solar velocity relative to distant galaxies [Hart and Davies, 1982].

plane (i.e., at $\lambda = 89^\circ$ and $\lambda = 269^\circ$). Excluding the contribution of resolved sources, the average surface brightness for the band within 24° of the ecliptic equator has been determined as a function of ecliptic longitude. Deviations from isotropy so obtained are represented in Figure 13.

The circle shown in Figure 13 represents isotropy. Percentage deviations up to about one percent are here plotted as a function of ecliptic longitude (λ). Each interval corresponds to a region of about 8×10^2 square degrees for which the average surface brightness is determined to a statistical uncertainty (one sigma) of 0.1% to 0.2%, arising from photon counting noise; the root

LARGE-SCALE SURFACE BRIGHTNESS VARIATIONS
HEAO-1 A2 X-RAY BAND I

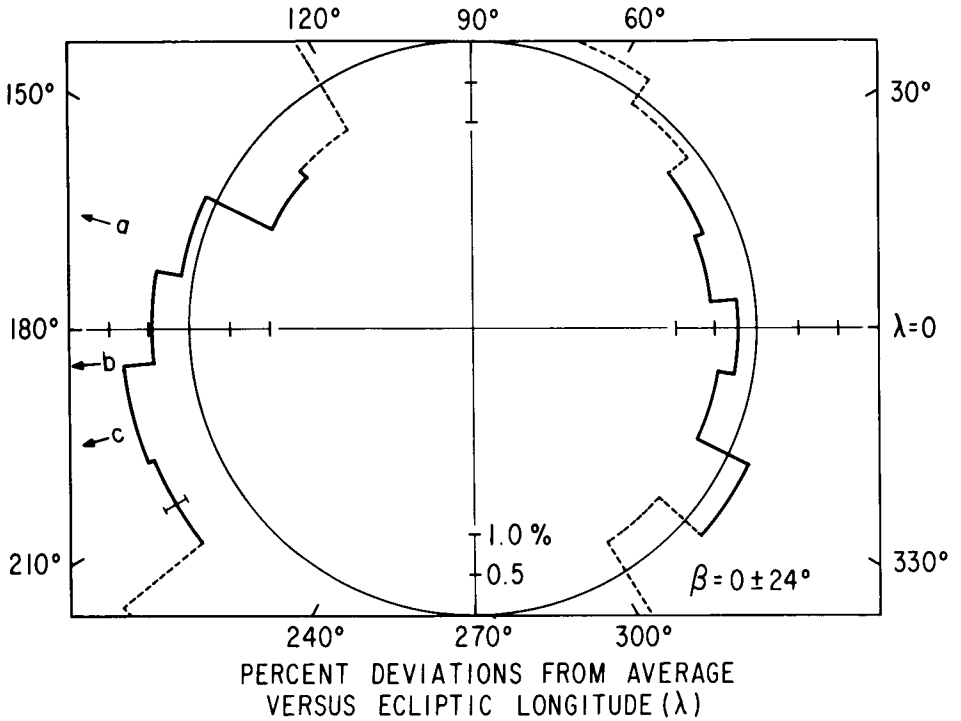


Figure 13. Percentage deviations from isotropy (represented by the circle) for the average surface brightness near the ecliptic plane ($\beta = -24^\circ \rightarrow +24^\circ$) as a function of ecliptic longitude (λ). Data obtained with HED units of HEAO-1 (A2) in all-sky survey. The one-sigma error bar shown corresponds to photon counting statistics. Special directions indicated are for the microwave dipole anisotropy results of Smoot et al. [1977] denoted by (a) and Cheng et al. [1979] denoted by (b), and the longitude where the supergalactic plane crosses the ecliptic equator (c). Surface brightness deviations for those ecliptic longitudes close to the galactic equator (i.e., near $\lambda = 89^\circ$ and $\lambda = 269^\circ$) are indicated with dashed lines.

mean squared (rms) fluctuation in apparent surface brightness among such intervals, due only to unresolved faint sources, is estimated to be about 0.3%. The galactic plane crosses the ecliptic equator at $\lambda = 89^\circ$ and $\lambda = 269^\circ$; those deviations in isotropy expected to be influenced most by this are shown as dashed lines. In this representation, the preferred directions of interest are:

- (a) the dipole anisotropy of the microwave background as determined by Smoot et al. [1977]
- (b) the dipole anisotropy of the microwave background as determined by Cheng et al. [1979]
- (c) the longitude where the plane of the Supergalaxy crosses the ecliptic equator

Considering only the solid portion of this plot, where galactic effects should be minimal, a weak residual large-scale asymmetry of the CXB becomes evident, one that repeats for independent sky surveys carried out with HEAO-1 at six-month centers.

Within estimated errors, the motion of the Sun relative to the backdrop of galaxies extending out to 70 Mpc [Hart and Davies, 1982] is consistent with the velocity vector inferred from a Compton-Getting [1935] interpretation of the dipole anisotropy observed for the cosmic microwave background. Based upon data from the HEAO-1 A2 cosmic X-ray experiment, the large-scale anisotropy of the CXB also appears to be compatible with such an interpretation [Shafer, 1983; Shafer and Fabian, 1983]. Considering the relatively large uncertainties involved, however, the anisotropy of the CXB is also consistent with an interpretation based on a possible component of the extragalactic background correlated with a direction defined by the physical center of the Supergalaxy [Boldt, 1981; Shafer, 1983], at the supergalactic longitude (104°) associated with the Virgo Cluster. Furthermore, the amplitude of large-scale variations in the X-ray background associated with the Milky Way at high galactic latitudes might not be small in magnitude relative to the anisotropy attributed to the extragalactic background [Iwan et al., 1982]. In order to obtain a diagnostic of these possible complications, we postulate that the dipole

anisotropy of the cosmic microwave background provides a precise indication of the direction of the observer's velocity relative to the proper (co-moving) frame of the CXB and examine the energy dependence of the fore-aft asymmetry of the X-ray background relative to this direction as a reference (see Figure 14).

The fore-aft asymmetry arising from the observer's velocity v/c (in units of the velocity of light) relative to the proper frame of an isotropic background of electromagnetic radiation having a spectrum of the form used here for the CXB is given by:

$$\Delta I/I = (v/c)[1 + \cos(\delta)] [3 + \alpha + (E/B)]$$

where δ is the half-cone angle defining the two opposite regions of the sky relative to the axis of motion; for the total CXB, $\alpha = 0.29$ and $B = 40$ keV. It is important to note that this Compton-Getting asymmetry increases with photon energy, becoming most pronounced for $E > B$. On the other hand, if there is a spatial inhomogeneity in the emission responsible for a background component characterized by a spectrum that is softer than the overall background (e.g., thermal emission with $kT < 40$ keV), then the corresponding asymmetry in the background flux would decrease with photon energy. In fact, we already know of two such X-ray background components characterized by $kT < 40$ keV. In particular, the unresolved galactic emission ($E > 3$ keV) at high latitudes may be described with $kT = 9$ keV [Iwan et al., 1982] and the background component due to clusters of galaxies may be characterized by $kT = 7$ keV [Stottlemyer and Boldt, 1984].

Corresponding to Figure 14 the ratio (R) of the fore-aft asymmetry for the band (10.3 – 20) keV to that for the band below 10.3 keV is given by $R = 1.72(+0.40, -0.40)$. This value for R (considering two-sigma statistical uncertainty) is compatible with the Compton-Getting effect as an explanation for the observed asymmetry (see Figure 14) but is incompatible with an explanation based on any anisotropic thermal background components having $kT \leq 9$ keV. However, an anisotropy in the foreground distribution of faint

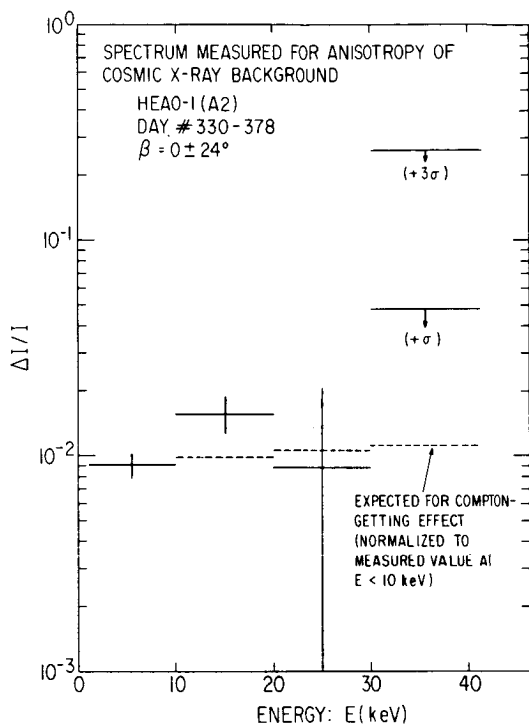


Figure 14. The fore-aft asymmetry ($\Delta I/I$) of the cosmic X-ray background, as measured with the HEAO-1 (A2) experiment, is exhibited as a function of photon energy E (keV). The reference direction is that defined by ecliptic coordinates: β (latitude) = 0° and λ (longitude) = 178° , corresponding to δ (declination) = 1° and a (right ascension) = 178° . The average surface brightness for a region $48^\circ \times 48^\circ$ ($\Delta\beta \times \Delta\lambda$), centered on the reference direction, is compared with that for an equivalent region in the opposite direction. Resolved sources, brighter than 2.1×10^{-11} ergs cm^{-2} s^{-1} (2-10 keV), have been excluded in the sample analyzed. Data were obtained with xenon gas proportional counters (high energy detectors HED-I and HED-III) and an argon counter (MED: medium energy detector) during the 48-day interval when great-circle scans with HEAO-1 covered the regions of the sky considered here. The one-sigma errors shown correspond to photon counting statistics. Dashed lines indicate the asymmetry expected for the Compton-Getting effect (normalized to the value measured for the band 1.3-10.3 keV).

unresolved extragalactic sources (e.g., correlated with the Supergalaxy), exhibiting spectral indices $\alpha \leq 0.7$, can not now be ruled out as a major cause of the asymmetry observed for the CXB.

The absolute precision of the CXB asymmetry measured with HEAO-1 (A2) below about 20 keV is limited by fluctuations in apparent surface brightness arising from unresolved faint foreground sources and not by the number of photons detected (i.e., this is the case for the two lowest energy bins exhibited in Figure 14). If the surface brightness measured could be isolated to those small pixels (i.e., of arc-minute size) devoid of foreground sources [down to a level corresponding to the limiting sensitivity S_0 of the HEAO-2 Einstein Observatory; Giacconi et al., 1979b], then the large-scale CXB anisotropy could be determined to a precision comparable with that for the cosmic microwave background. In this way, the CXB could be used for determining the vector velocity of the co-moving frame in which to examine anisotropies *intrinsic* to the cosmic microwave background, an issue that is central to the observational basis of modern cosmology.

5. OUTLOOK

The residual CXB needs to be measured directly; this will involve resolving out discrete sources in the background. The magnitude and fluctuations expected for the integral contribution of these individual sources to the CXB at any given energy band may be obtained from the corresponding $\log(N)$ - $\log(S)$ relation that describes the counts of such sources. It is usual to characterize this relation by an index γ , generally a weak function of S , defined by

$$\gamma(S) = -d[\log(dN/dS)]/d[\log(S)].$$

For Euclidean space $\gamma = 2.5$. For the case of non-evolving sources (i.e., constant co-moving density and invariant source characteristics) standard cosmological models have $\gamma = 2.5$ only for the brightest (nearest) sources, with γ becoming smaller as S decreases. Since the extragalactic foreground sources detected with HEAO-2 exhibit a $\log(N)$ - $\log(S)$ relation consistent with

$\gamma = 2.5$ (i.e., $N \propto S^{-1.5}$) all the way down to the Einstein Observatory's survey limit (S_0), we must consider the effects of evolution. Limiting the HEAO-2 sample to AGN alone yields $\gamma = 2.71(+.15, -.15)$, indicating that this evolution is probably substantial [Gioia et al., 1984]. By contrast, the number-flux relation for the subsample made up of clusters of galaxies is characterized by $\gamma = 2.04(+.23, -.23)$, less than the Euclidean value (as anticipated).

The AXAF (Advanced X-ray Astrophysics Facility) to be co-orbiting with the Space Station will have the capability of resolving hard X-ray sources (3-10 keV) contributing to the CXB. The sensitivity for detecting point sources with the AXAF focusing X-ray telescope is expected to be one to two orders of magnitude better than that for the HEAO-2 Einstein telescope [Zombeck and Ramage, 1983]. The fraction of the CXB yet to be resolved into discrete objects depends on the source number-flux relation at $S < S_0$; power law extrapolations using $\gamma = 2.5(+0.5, -0.5)$ are exhibited in Figure 15 for purposes of estimation. Assuming that the CXB point-source contribution to be resolved with the AXAF telescope arises mainly from AGN with canonical spectra ($\alpha = 0.7$) and that the number-flux relation persists to about $0.1S_0$ with $\gamma \geq 2$, we note that the resolved portion would be in excess of 35% (for the band 3-10 keV). Since the 3-10 keV spectrum of the CXB is significantly flatter than that of such AGN, however, their contribution over this band could not be this large [De Zotti et al., 1982]. As exhibited in Figure 15, the number of such resolved sources is expected to be much less than one per square arc-minute pixel.

Based on data from the imaging proportional counter in the focal plane of the Einstein Observatory telescope, Hamilton and Helfand [1986] have already investigated the surface brightness of the X-ray background (1-3 keV) with arc-minute resolution, thereby obtaining upper limits on small-scale fluctuations which suggest that the residual CXB could very well be predominantly diffuse. If due to point sources, they find that the number needed would have to exceed $5 \times 10^3 \text{ degree}^{-2}$, much larger than the estimated total number of quasars [Schmidt and Green, 1986]. Assuming that these sources are at $z \leq 4$ (with $\Omega = 1$) the residual CXB spectrum (see Figure 11) implies that their average X-ray luminosity would have to be less than $10^{45} \text{ erg s}^{-1}$. If these objects are precursor AGN whose thermal X-radiation is at a level close to the

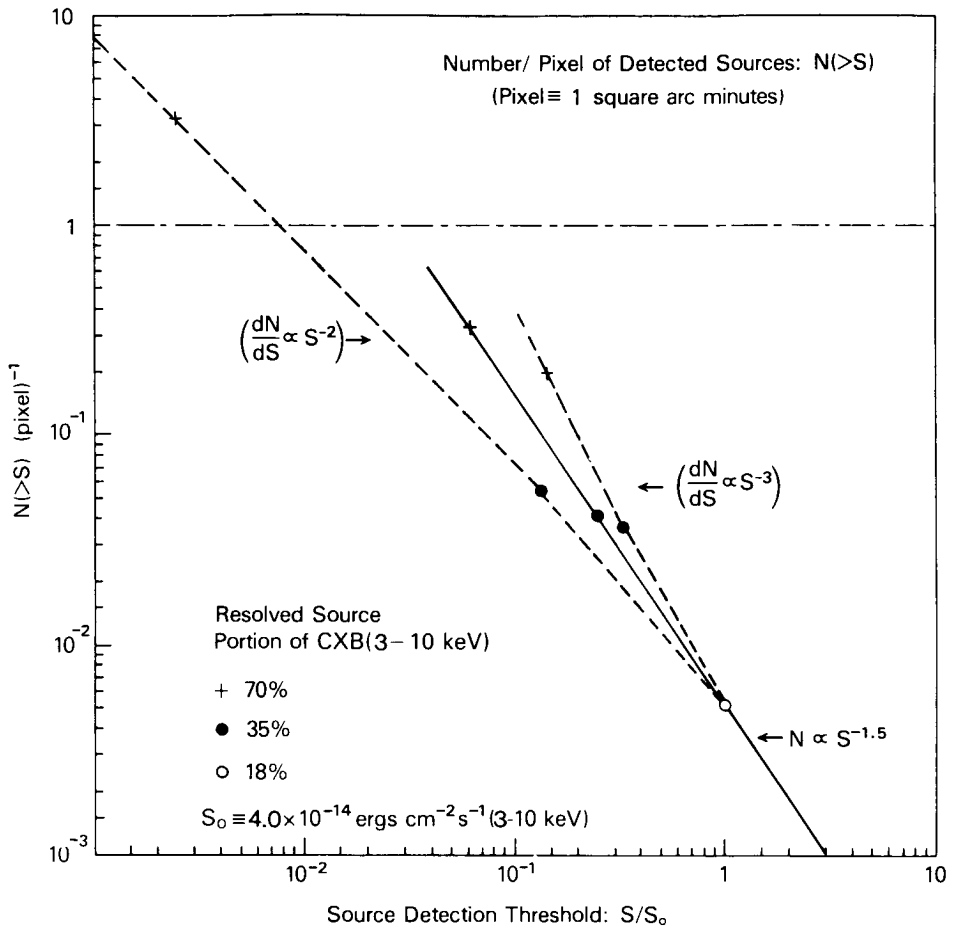


Figure 15. Extrapolation of source counts to $S/S_0 < 1$, normalized to HEAO-2 measurements at $S/S_0 > 1$ [Gioia et al., 1984]. Points designated by various symbols indicate corresponding percentage of the CXB resolved (3-10 keV), shown separately for $\gamma = 2, 2.5$ and 3 (see text). For an energy spectral; index $\alpha = 0.7$, S_0 (3-10 keV) = $4.0 \times 10^{-14} \text{ ergs cm}^{-2} \text{ s}^{-1}$ corresponds to S_0 (1-3 keV) = $2.6 \times 10^{-14} \text{ ergs cm}^{-2} \text{ s}^{-1}$ of the HEAO-2 deep survey [Giacconi et al., 1979b]. $N(>S)$, average number of sources per pixel brighter than S , is plotted versus S/S_0 . Pixel size is 1 square arc-minute.

Eddington luminosity limit (see Section 3), then the characteristic central compact mass involved has to be less than that measured for typical Seyfert galaxies in the present epoch [Wandel and Mushotzky, 1986], as expected.

Considering that a fraction (f) of the residual CXB over the band 3-10 keV (having the spectrum indicated in Figure 11) arises from a presently unknown population of faint discrete hard X-ray sources, their average flux would be given by

$$\langle S(3 \text{ keV}-10 \text{ keV}) \rangle = 2.6 \times 10^{-15}(f/N) \text{ ergs cm}^{-2} \text{ s}^{-1}$$

where N is the number of such objects per square arc-minute. For the average source in this population to be detectable with AXAF would require $N < (4f)$ per square arc-minute. This overall performance level is probably sufficient for the study of that particular candidate population of young precursor AGN sources already postulated for the residual CXB [Leiter and Boldt, 1982]. The portion $(1-f)$ of the residual CXB unresolved with AXAF (e.g., due to a diffuse component) would yield a photon flux density at the focal plane of the telescope equal to $1.4 \times 10^{-5}(1-f) \text{ mm}^{-2} \text{ s}^{-1}$ for the band 3-10 keV. Since the internal background for imaging X-ray detectors over this energy band is generally on the order of $10^{-5} \text{ mm}^{-2} \text{ s}^{-1}$ or greater, unresolved and/or diffuse components of the residual CXB may not be very well suited for study with the AXAF telescope. "Faster" optics are desirable for such weak surface brightness investigations, but the angular resolution might not need to be better than an arc-minute for isolating those pixels to be studied which are devoid of foreground point sources (see Figure 15).

If the residual CXB is dominated by point sources having $S > 0.01S_0$, then they will be detectable with AXAF and their average spectrum can be determined. As shown by Worrall and Marshall [1984], based on HEAO-1 data, the residual CXB spectrum over the band 3-10 keV is clearly incompatible with $\alpha > 0.68$ (i.e., the 90% confidence lower limits to the spectra index characterizing their quasar sample). Over this band suitable to AXAF, the sources of the residual CXB should exhibit an average spectrum with $\alpha = 0.29$ (see Figure 16), indicating a population of objects that are distinct from

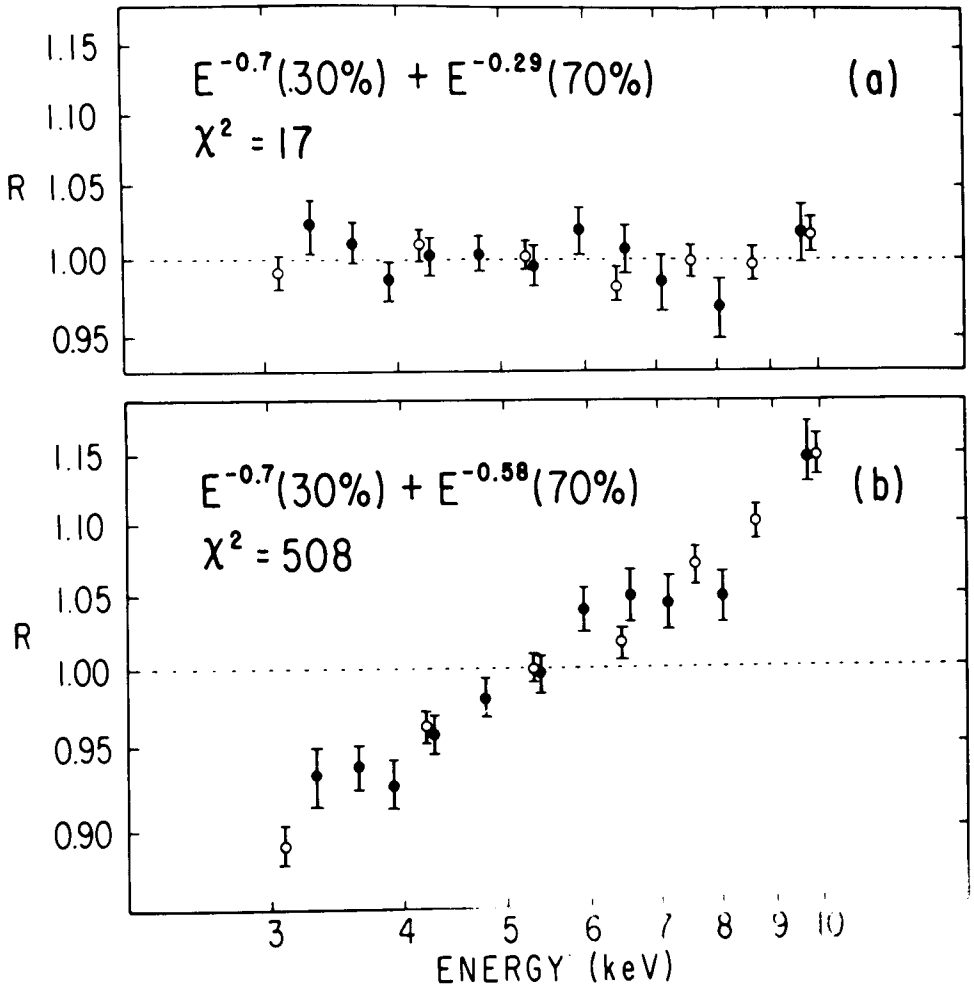


Figure 16. The ratio (R) of observed counts for the X-ray background to those predicted (3-10 keV) for combinations of incident power law spectra [Worrall and Marshall, 1984]. Open circles are measurements with the HEAO-1 (A2) HED-1 detector. Closed circles are with the MED.

the AGN X-ray sources already studied (see Figure 6). This would be consistent with the conclusion reached by Narlikar and Burbidge [1983] who, considering the upper limit to the extragalactic night sky background light, find it to be unlikely that canonical quasar-like objects dominate the CXB (i.e., the ratio of X-ray to optical emission must be extraordinarily large for the principal sources of the CXB).

If much of the residual CXB is due to a hot IGM, then there would be spatial structure to this sky background on a scale defined by the clumping of the gas. In this connection we note that the large-scale structures associated with galaxy clustering in recent epochs (e.g., superclusters, giant voids) may be remnant indicators of the distribution of relatively young matter at the epoch of galaxy formation [Oort, 1983]. Assuming a present-epoch scale $\simeq 0.04$ (c/H_0), as described by Bahcall and Burgett [1986], the related structure at any epoch would appear to us with an angular scale greater than the field of view (\sim one degree) of the AXAF telescope.

Direct measurements of the residual CXB over a bandwidth sufficiently large to cover the spectrum (i.e., $\Delta E > B$) are beyond the capability of already developed focusing X-ray optics. The sensitive all-sky survey of soft X-rays (< 2 keV) to be provided by the focusing X-ray telescope of the forthcoming Roentgen Satellite (ROSAT) [Trumper, 1984] is likely to be complicated by galactic emission. Although the precise direction to be associated with the dipole anisotropy of the residual CXB (up to 10 keV) could be obtained via an all-sky scan with a broadband "fast" focusing X-ray telescope [such as developed by Serlemitsos et al., 1984], a verification of the Compton-Getting velocity interpretation would still require examining how the anisotropy varies at substantially higher energies.

REFERENCES

- Alexander, J., and Clark, T., 1974, in *High Energy Particles and Quanta in Astrophysics*, ed. F. McDonald and C. Fichtel (Cambridge: MIT Press), pp. 299-300.
- Bahcall, N., and Burgett, W., 1986, *Astrophys. J.*, **300**, L35.

Bignami, G., Fichtel, C., Hartman, R., and Thompson, D., 1979, *Astrophys. J.*, **232**, 649.

Boldt, E., 1971, *Bull APS*, **224**, 534.

Boldt, E., 1974, in *High Energy Particles and Quanta in Astrophysics*, ed. F. McDonald and C. Fichtel (Cambridge: MIT Press), pp. 401-406.

Boldt, E., 1981, *Comments Ap.*, **9**, 97.

Boldt, E. et al., 1979, in (COSPAR) *X-ray Astronomy*, ed. W. Baity and L. Peterson (Oxford: Pergamon Press), p. 433.

Boldt, E., and Leiter, D., 1984, *Astrophys. J.*, **276**, 472.

Bookbinder, J. et al., 1980, *Astrophys. J.*, **237**, 647.

Cheng, E. et al., 1979, *Astrophys. J.*, **232**, L139.

Clark, T., Brown, L., and Alexander, J., 1970, *Nature*, **228**, 847.

Code, A., and Welch, G., 1982, *Astrophys. J.*, **256**, 1.

Compton, A., and Getting, I., 1935, *Phys. Rev.*, **47**, 817.

de Vaucouleurs, G., 1958, *Astrophys. J.*, **63**, 253.

De Zotti, G. 1982, *Acta. Cosmol.*, **11**, 65, "Second International Krakow School of Cosmology", Jablonna, Poland.

De Zotti, G. et al., 1982, *Astrophys. J.*, **253**, 47.

Dube, R., Wickes, W., and Wilkinson, T., 1979, *Astrophys. J.*, **232**, 333.

Elvis, M., 1985, in Proc. Japan/U.S. Symp. (Jan. 1985), eds. Y. Tanaka and W. Lewin (Tokyo: Inst. Space Astron. Sc.), p. 291; CFA Preprint #2126.

- Elvis, M., Wilkes, B., and Tananbaum, H., 1985, *Astrophys. J.*, **292**, 357.
- Elvis, M., Soltan, A., and Keel, W., 1984, *Astrophys. J.*, **283**, 479.
- Fabian, A., 1981, Proc. Tenth Texas Symp. Rel. Astr., *Ann. N.Y. Acad. Sci.*, **375**, 235.
- Fichtel, C., Simpson, G., and Thompson, D., 1978, *Astrophys. J.*, **222**, 833.
- Fichtel, C., and Trombka, J., 1981, *Gamma Ray Astrophysics*, NASA SP-453.
- Garmire, G., 1979, in *HEAO Science Symposium*, ed. C. Dailey and W. Johnson, NASA CP-2113, p. 49.
- Giacconi, R., 1986, this volume.
- Giacconi, R., Gursky, H., Paolini, F., and Rossi, B., 1962, *Phys. Rev. Letters*, **9**, 439.
- Giacconi, R., Gursky, H., and van Speybroeck, L., 1968, *Ann. Rev. Astron. Astrophys.*, **6**, 373.
- Giacconi, R. et al., 1979a, *Astrophys. J.*, **230**, 540.
- Giacconi, R. et al., 1979b, *Astrophys. J.*, **234**, L1.
- Gioia, I. et al., 1984, *Astrophys. J.*, **283**, 495.
- Gruber, D., Rothschild, R., Matteson, J., and Kinzer, R., 1984, in *Conf. Proc. X-ray and UV Emission From Active Galactic Nuclei*, ed. W. Brinkman and J. Trumper (Garching: Max Planck Institute), p. 129.
- Guilbert, P., and Fabian, A., 1986, *MNRAS*, **220**, 439.
- Hamilton, T., and Helfand, D., 1986, *Astrophys. J.*, submitted.
- Hart, L., and Davies, R., 1982, *Nature*, **297**, 191.

Holt, S., 1974, ed. Proc. GSFC Workshop Electron Contam. X-ray Astron. Exp., GSFC X-661-74-130.

Iwan, D. et al., 1982, *Astrophys. J.*, **260**, 111.

Joubert, M. et al., 1983, *Astron. Astrophys.*, **128**, 114.

Leiter, D., and Boldt, E., 1982, *Astrophys. J.*, **260**, 1.

Maccacaro, D., Gioia, I., and Stocke, J., 1984, *Astrophys. J.*, **283**, 486.

Malkan, M., and Sargent, W., 1982, *Astrophys. J.*, **254**, 22.

Marshall, F. et al., 1980, *Astrophys. J.*, **235**, 4.

Maxon, S., 1972, *Phys. Rev. A.*, **5**, 1630.

McCammon, D. et al., 1983, *Astrophys. J.*, **269**, 107.

McKee, J. et al., 1980, *Astrophys. J.*, **242**, 843.

Mushotzky, R., 1982, *Astrophys. J.*, **256**, 92.

Mushotzky, R., 1984, *Adv. Space Res.*, **3**, 157.

Narlikar, J., and Burbidge, G., 1983, *Astron. Astrophys.*, **118**, 154.

Oort, S., 1983, *Ann. Rev. Astron. Astrophys.*, **21**, 373.

Osmer, P., 1982, *Astrophys. J.*, **253**, 28.

Ostriker, J., and Cowie, L., 1981, *Astrophys. J.*, **243**, L127.

Paresce, F., McKee, C., and Bowyer, S., 1980, *Astrophys. J.*, **240**, 387.

Persic, M. et al. 1986, in preparation.

- Peterson, L., 1975, *Ann. Rev. Astron. Astrophys.*, **13**, 423.
- Piccinotti, G. et al., 1982, *Astrophys. J.*, **253**, 485.
- Razin, V., 1960, *Izv. Vysshikh Uchebn. Zacedenii, Radiofiz.*, **3**, 584.
- Rothschild, R. et al., 1979, *Sp. Sci. Instr.*, **4**, 269.
- Rothschild, R. et al., 1983, *Astrophys. J.*, **269**, 423.
- Schmidt, M., and Green, R., 1983, *Astrophys. J.*, **269**, 352.
- Schmidt, M., and Green, R., 1986, *Astrophys. J.*, **305**, 68.
- Segal, I. E., 1983, *Phys. Rev. D.*, **28**, 2393.
- Segal, I. E., 1985, in *Cosmic Background Radiation and Fundamental Physics*, Proc. Third Rome Meeting on Astrophysics, ed. F. Melchiorri (Bologna: Italian Physical Society), p. 209.
- Serlemitsos, P. et al., 1984, *IEEE Trans. Nucl. Sci.*, **NS-31**, 786.
- Shafer, R., 1983, Ph.D. dissertation, University of Maryland, NASA TM 85029.
- Shafer, R., and Fabian, A., 1983, in *Early Evolution of the Universe and its Present Structure*, ed. G. Abell and G. Chincarini (IAU), **104**, 333.
- Simon, A., 1977, in *Radio Astronomy and Cosmology*, ed. D. Jauncey (Dordrecht: D. Reidel Publishing Co.), p. 349.
- Smoot, G., Gorenstein, M., and Muller, R., 1977, *Phys. Rev. Letters*, **39**, 898.
- Stottlemyer, A., and Boldt, E., 1984, *Astrophys. J.*, **279**, 511.
- Toller, G., 1983, *Astrophys. J.*, **266**, L79.

Trombka, J. et al., 1977, *Astrophys. J.*, **212**, 925.

Trumper, J., 1984, *Phys. Scripta*, **T7**, 209.

Tucker, W., 1984, *The Star Splitters*, NASA SP 466.

Turner, E., and Geller, M., 1980, *Astrophys. J.*, **236**, 1.

Wandel, A., and Mushotzky, R., 1986, *Astrophys. J.*, **306**, L61.

Weiss, R., 1980, *Ann. Rev. Astron. Astrophys.*, **18**, 489.

Weller, C., 1983, *Astrophys. J.*, **268**, 899.

Worrall, D., and Marshall, F., 1984, *Astrophys. J.*, **276**, 434.

Zombeck, M., and Ramage, S., 1983, "Counting Rates For Representative AXAF Imaging Instruments" (Cambridge: Smithsonian) SAO-AXAF-83-017.